Characterization of Fragility in Silica-Based Ionogels

Patricia Mcneil, Thibaud Guillemin, Maggie Fox, Jean Le Bideau, Bruce Dunn

Characterization of Fragility in Silica-Based Ionogels

Patricia McNeil, Department of Materials Science and Engineering, University of California, Los Angeles, California 90095, USA
Thibaud Guillemin, Nantes Université, CNRS, Institut des Matériaux de Nantes Jean Rouxel, IMN, F-44000 Nantes, France
Maggie Fox, Department of Materials Science and Engineering, University of California, Los Angeles, California 90095, USA
Jean Le Bideau, Nantes Université, CNRS, Institut des Matériaux de Nantes Jean Rouxel, IMN, F-44000 Nantes, France
Bruce Dunn*, Department of Materials Science and Engineering, University of California, Los Angeles, California 90095, USA
Email: BDunn@ucla.edu

Abstract
The present study examines the ionic conductivity and transport properties for ionic liquids confined within mesoporous materials. The fragility index was determined for several samples with varying microstructures and used to characterize performance as a pseudosolid electrolyte. The degree of microstructure complexity was characterized via the mass fractal dimension, which correlates with the fragility index in the pore size domain studied. We demonstrate for the materials studied here that the presence of the microporous matrix serves to inhibit ion mobility, and as the complexity of the matrix increases, the fragility index also increases, leading to lower conductivity materials. The microstructural features influencing conductivity were examined using Archie's law when assuming the matrix conductivity to be negligible. This type of analysis, previously validated for rock matrices, has now been extended to pseudosolid electrolyte materials. The results indicate that ionogel samples can approach the conductivity of the unconfined ionic liquid. These conclusions are applicable to a variety of pseudosolid electrolyte systems and have important implications for the design of electrochemical devices.

Introduction

The design of electrolytes exhibiting liquid-like transport properties with the form and structure of a solid separator is a promising direction for the development of solid-state electrochemical devices, (1−3) especially solid-state batteries and supercapacitors, where sufficiently high conductivities and device reliability are major concerns. (4−6) Determining the fundamental transport properties for these structures is critical in the development and optimization for such devices. In recent years, pseudosolid-state electrolytes known as ionogels have emerged as a group of solid-phase materials that exhibit the properties of ionic liquids. These materials, which are comprised of two interpenetrating phases, can be synthesized using well-known room-temperature sol–gel synthesis methods which produce complex open microstructures with various dimensionalities. Ionogels with host matrix made only of silica are macroscopically rigid but exhibit liquid-like transport properties due to an ionic liquid (IL) being confined in the pores of a sol–gel-derived matrix. Typically ionogels contain 60–90% IL by volume which, in contrast to sol–gel materials that use volatile solvents (e.g., alcohols), is retained in the final material because of the extremely low volatility of ILs. (7) The IL can be introduced either during the sol–gel process (4,8−10) or after matrix synthesis via infiltration. (5,11) By confining the IL in the mesoscale pores of the sol–gel matrix, ionogels take full advantage of ionic liquid utility, including good chemical stability, high ionic conductivity, thermal stability, and a wide electrochemical window, (7,12−14) in combination with a rigid solid backbone. Here, we determine how the nanoscale structure in an ionogel influences its performance as a pseudosolid electrolyte, where the performance parameters are the fragility and the conductivity.

Fragility is a measure of the thermal sensitivity of the liquid structure and is described by the fragility index D. (11,15,16) A fragile liquid collapses under weak perturbations and leads to structural rearrangement. Thus, a fragile liquid exhibits fast dynamical rearrangement characterized by short relaxation times and non-Fickian diffusion, giving rise to non-Arrhenius behavior. (17) A low D value corresponds to weak molecular interactions, while a high value corresponds to strong molecular interactions. In this way, fragility is related to molecular mobility with its correlative effect on ionic conductivity and viscosity: a small D value implies a high ionic mobility and a low viscosity, i.e., a high fragility. In ILs, the interaction between ions results in their high cohesive energy. The confinement of ILs in proximity to polar silica surfaces (silanols with multiple orientations forming dynamic hydrogen bonds) is known to produce layering with either cations or anions preferentially interacting with the surface. (11) In the present work, we use the fractal dimensionality of the silica network to characterize the relationship between the microporosity and the fragility of the ionogel and determine its influence on ion transport properties.

The fragility of ionogels arises from interactions between the confined liquid and the silica matrix, features which can be analyzed by characterizing the nature of the microstructure in terms of pore volume, pore size distribution, and fractal dimensionality. Although the pore sizes in the matrix dictate the degree of confinement and the pore volume determines the relative fraction of conducting medium, neither parameter captures entirely the complexity of transport in ionogels. For this reason, we utilize the mass fractal dimension D_f to describe how mass M is distributed in a porous material of size L according to eq 1 (18)

$$M \propto L^{D_f} \tag{1}$$

Sol–gel preparation approaches lead to different values of D_f for silica matrices because of the wide range of synthesis conditions. On the basis of synthesis parameters such as the concentration of precursors, the pH for catalysis, and the relative reaction rates for hydrolysis and condensation, silica aggregates will form from a colloidal suspension, generating spherical particles often at the nanoscale. These aggregates function as the building blocks to form the self-similar fractal structure. The conditions for gel network formation effectively determine the level of complexity in the gel backbone which is then expressed as the mass fractal dimension. For example, a gel approaching $D_f = 3$ has a highly complex and branched microstructure in contrast to a gel of $D_f = 2$ which is more chain like. (18) In this way, one can establish how the fractal dimension relates to the fragility index, where more complex networks correspond to poor diffusion at the macroscopic scale.

Molecular interactions within the pore fluid are readily characterized by measuring the ionic conductivity as a function of temperature. When ln(σ) is plotted versus 1000/T, the trend can be fitted with the Vogel–Tamann–Fulcher equation expressing the conductivity σ (S cm^{-1}) of liquids with non-Arrhenius behavior

$$\sigma = \sigma_0 e^{-B/T-T_0} \tag{2}$$

where σ_o (S cm^{-1}) is the conductivity at infinite temperature, T_o (K) is the ideal glass transition temperature, and B (K) is related to the activation energy. The fragility index D is then obtained following the equation

$$D = \frac{B}{T_0} \tag{3}$$

The fragility index in eq 3 expresses the thermal sensitivity of the liquid inside the structure, which can then be combined with microstructure analysis for ionogels to establish a relationship between the silica matrix and the conductivity of the ionic liquid. (15,16)

Modeling the ionic conductivity of ionogels with differing microstructures must take into account the interactions between the pore fluid and the confining matrix. To some degree, this approach has been explored extensively in the geophysical sciences. Naturally occurring porous media such as reservoir rocks have been shown to demonstrate fractal geometries like ionogels but with porosities less than φ = 0.5. It is well known that the solid matrix greatly influences many transport properties, including the diffusion, hydraulics, and conductivity of the pore fluid by modifying the tortuosity of the pathway. (19) Archie's law represents the classic empirical representation of this concept in fully saturated porous media

$$F \equiv \frac{\sigma_w}{\sigma} = a\phi^{-m} \tag{4}$$

where the formation factor, F, represents the effect of the presence of the confining matrix, which is assumed to have negligible electrical conductivity. The formation factor is defined as the ratio of the electrical conductivity of the pore fluid, σ_w, and the observed electrical conductivity, σ. The formation factor has a power law relationship with porosity φ ($0 < \varphi < 1$), where a and m are the tortuosity and cementation constants, respectively. The cementation constant, which describes the strength of the effect of the matrix on the pore fluid transport properties, has a theoretical limit between 1 for very direct pathways and 3 for very complex pathways. F typically ranges from 10 to 100 for various sandstones, which are the naturally occurring porous matrices most often studied. (20,21) The derivation of Archie's law from Maxwell–Wagner theory (see Supporting Information S1) indicates that the interface between two materials with different relaxation times results in charge accumulation. (19,20)

A full analysis for conduction within the ionogel would be incomplete without considering the tortuosity resulting from the matrix microstructure. Another statement of Archie's law represents the formation factor directly in terms of tortuosity

$$F = \frac{\phi}{T} \tag{5}$$

where $T = L_T/L_o$, L_T is a transport length through a tortuous pathway, and L_o is the macroscopic straight-line length. (19) The more complex the microstructure of the confining matrix, the higher the tortuosity, which results in more difficult ionic transport.

The tortuosity (τ_e) can be expressed in terms of a random walk fractal dimension, D_w (>2). In this representation, for a random walker taking N steps, the root mean squared distance traveled has the relationship $N \approx L^{D}_{W}$. (22) Then, using Einstein's relation between the electrical conductivity and the diffusion coefficient, the tortuosity is given as a power law (19)

$$\tau_e = \phi^{D_w-2/D_f-E} \tag{6}$$

where D_f is the mass fractal dimension and E is the Euclidian dimension, which is 3 for a three-dimensional space. Here, $0 < D_f < E$, so the scaling exponent will be negative, indicating that as the porosity increases, the tortuosity decreases. For unconfined pore fluid, the porosity approaches 1 and the tortuosity also approaches 1, indicating $L_T = L_o$. Although work has also been done to simulate random walks in porous media, (23−25) some attempts have been made to simplify the relationship between D_w and D_f,

showing that for percolation clusters, the ratio of D_w to D_f tends to a constant which is related to the number of distinct sites $S(N)$ that a random walker can visit along the substrate (Supporting Information S2). (23,26)

The difficulties in quantifying analyses based on a random walk fractal dimension have resulted in simplified descriptions for tortuosity. One common way of describing tortuosity in porous media is by modeling a network of streamtubes, which can be thought of as direct pathways within the pore structure. This approach utilizes a tortuosity fractal dimension, D_T, so that the transport length can be described as

$$L_T(\varepsilon) = \varepsilon^{1-D_T} L_o^{D_T} \tag{7}$$

where ε is the measurement length scale. (27) Although the fractal streamtube representation of tortuosity has been validated in porous rocks (27,28) and yielded analytical models for electrical conductivity, (20) it is ineffective at describing conductivity in matrices with porosities greater than φ = 0.5. For such high porosity levels, the extremely open nature of the matrix no longer assumes the streamtube geometry. (29) In the present study, we use fragility-based concepts to identify microstructure features which lead to high ionic conductivity for ionogels with porosities ranging from φ = 0.7 to 0.9. Understanding ionogel performance, specifically the interplay between a resistive complex matrix and ionic liquid mobility, is key to developing guidelines for the design of pseudosolid electrolytes.

Experimental Methods

Ionogel Synthesis and Preparation

In this work, highly porous silicas (between 67% and 91% porosity) are used as the host materials for 1-ethyl-3-methylimidazolium bis(trifluoromethylsulfonyl)imide (EMImTFSI) ionic liquid (Solvionic, 99.9% purity). The mesoporous silica network was synthesized by an ambient drying procedure in which complex micro/mesoporous pore structures of silica were prepared using an acid–base-catalyzed sol–gel synthesis. (30) First, a sol of tetraethyoxysilane (TEOS) (Sigma-Aldrich), methyl triethyoxysilane (MTES) (Sigma-Aldrich), deionized water, ethanol (EtOH), formamide (Sigma-Aldrich), and concentrated HCl (Sigma-Aldrich) was mixed at a molar ratio 1.5:1:6.25:6.25:5 mol of TEOS:MTES:EtOH:H_2O:formamide. Then, a base catalyst of 2 M NH_4OH was added at a volume ratio of 6 mL of base to 17 mL of sol before transferring to a 10 cm × 10 cm × 1.5 mm plastic mold. After aging for 2 days, gel monoliths were removed from the cassettes and submerged in ethanol. The ethanol was then exchanged with *n*-heptane, which is the final drying solvent. Many of the samples were also washed with a 0.5–2% volume of trimethylchlorosilane (TMCS) in heptane for 30 min, which functioned as a surface modification to generate a hydrophobic surface. These samples were rinsed in ethanol to remove byproducts of the chlorosilane reaction with silica and dried in a heptane-rich atmosphere. The resulting samples were dried at ambient temperature and pressure by draining the solvent and allowing slow evaporation of the pore solvent in a sealed container over ∼1 week. Finally, some of these "ambigel" monoliths were heated for 5 h at 500 °C in static air to remove any organic phase. Table 1 summarizes the processing parameters used to achieve a wide range of microstructures and porosities.

Table 1. Physical Properties of Ambigel Samples Prepared under Varying Synthesis Conditions[a]

sample no.	description	fractal dimension (D_f)	fragility index (D)	thickness (mm)	porosity	BET surface area (m^2/g)	total pore volume (cm^3/g)	fraction of microporous volume
1	2 vol % TMCS, calcined	2.1	3.5 ± 0.2	1.2	87%	1002	3.15	0.23
2	2 vol % TMCS calcined	2.2	3.2 ± 0.1	1.3	91%	817	3.94	0.14
3	2 vol % TMCS	2.2	3.8 ± 0.2	1.3	90%	1288	2.94	0.34
4	0.5 vol % TMCS	2.3	3.8 ± 0.1	1.2	80%	790	1.69	0.35
5	0.5 vol % TMCS calcined	2.4	3.6 ± 0.2	1.1	91%	991	4.36	0.16
6	no TMCS	2.4	3.7 ± 0.2	0.9	73%	1257	1.66	0.69
7	1 vol % TMCS	2.4	4.3 ± 0.2	1.1	85%	1244	2.26	0.43
8	no TMCS calcined	2.5	4.6 ± 0.2	0.8	67%	882	0.78	0.88

[a]Surface modifications with TMCS were utilized to achieve a variety of porosity and fractal dimension ranges. Calcination ensured the surface homogeneity of the silica matrix for these samples.

After sol–gel synthesis, ionogels were obtained by infiltrating an ionic liquid into the highly porous silica matrix. Silica samples of 30–50 cm2 were dried at 50 °C under moderate vacuum overnight to ensure the absence of water. Under inert atmosphere, EMImTFSI ionic liquid was dropped on the silica samples. After 3 days, the silica matrix was considered fully filled with the ionic liquid when the mass was unchanged. At this point, the samples were perfectly transparent in contrast to their opacity prior to impregnation. Ionic liquid excess was removed by wiping.

Structural Characterization and Mass Fractal Dimension

Low-temperature nitrogen sorption was measured on a surface area and porosity analyzer (ASAP2020 Plus, Micromeritics Instruments Corp., Norcross, GA). Specific surface area, micro- and mesopore volumes, pore size distribution, and vol % open porosity were calculated as described in the 2015 IUPAC Technical Report. (31) The fraction microporosity was also calculated and is described in the Supporting Information (S3). Nitrogen porosimetry isotherms were used to determine the surface fractal dimension, Ds, which should be equal to the mass fractal dimension in fractal solids, (30,32,33) utilizing the Frenkel–Halsey–Hill method

$$\ln n = C - (3 - D_s)\ln\left(RT \ln \frac{P_0}{P}\right) \tag{8}$$

where n is the quantity of N2 gas adsorbed in cm3 STP g–1, P is the pressure, and P0 is the saturation vapor pressure. (34) Sample calculations are given in the Supporting Information (S4).

Conductivity Measurements and Fragility Index

Ionogels were placed in a Swagelok cell between two stainless steel polished electrodes. Electrochemical impedance spectroscopy (EIS) measurements were performed on the cells every 10° C between −20 and 80 °C after 2 h of temperature stabilization. The EIS measurements used an amplitude of 20 mV between 100 mHz and 1 MHz. Conductivity (σ in S cm–1) values at a given temperature for each of the samples were obtained from the measured resistance according to eq 9

$$\sigma = \frac{e}{RS} \tag{9}$$

where e is the thickness of the sample (cm), S is the electrode area of the sample (cm2), and R is the measured resistance (Ω). The conductivity was then fitted with eq 2, and the fragility index was obtained with eq 3. Example calculations are provided in the Supporting Information (S5).

Results and Discussion

To establish the relationship between fragility and ionic conductivity, we must first analyze ionic liquid motion within a silica matrix and the means by which mobility is inhibited by the presence of the solid backbone. Silica samples used for IL infiltration are presented in Table 1, numbered from the lowest to the highest fractal dimension, which relates to increasing complexity of the silica matrix. Corresponding ionic conductivities are presented in Figure 1, ranging from values very close to nonconfined IL EMImTFSI (5.6 mS cm–1 at 20 °C) to more than one decade lower.

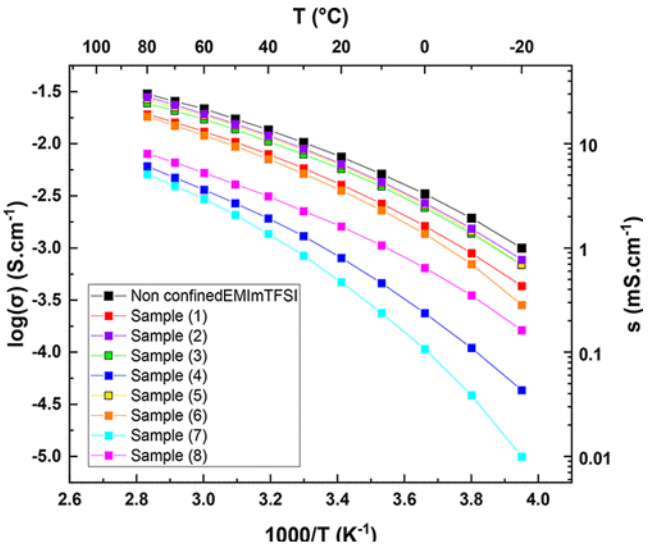

Figure 1. Ionic conductivities for ionogel samples over the range from −20 to 80 °C.
Ionogel samples were prepared using a variety of processing conditions, including surface modifications and gel calcination, to achieve a variety of porosities and fractal dimensions.

From Figure 1, ionic conductivity values were easily fitted (Figure S3) with the Vogel–Tamann–Fulcher equation (eq 3), thus enabling extraction of the fragility index. (15,16)

From Table 1 and Figure 2a, one observes the relationship between the fragility index and the fractal dimensionality, thus relating the ion dynamics in the ionic liquid to the degree of matrix complexity. A high fragility index could be linked either to strong molecular interactions or to poor macroscale diffusivity as would occur with the more complex networks that one associates with higher fractal dimensions. (11) For this reason, it is not surprising for the fragility index, D, to scale with the fractal dimension, Df (Figure 2a). This relationship enables us to determine the influence of pore volume. In Figure 2b, the pore size distribution is compared for samples 1 and 6, which represent high and low fractal dimension materials, respectively. High fractal samples frequently exhibit smaller pore size distributions and high surface areas to satisfy a complex distribution of mass in the microstructure. This behavior is observed in the pore volume and pore size distributions in Figure 2b. The decrease in pore volume, a result of smaller pore diameters, is characterized by an increase in fragility index (i.e., decrease of fragile behavior, Figure 2c) as a result of greatly decreased pore sizes. The increase in fragility index results in a lower ionic liquid electrolyte mobility as the silica network creates a more tortuous conduction pathway than that of unconfined ionic liquid electrolyte, as illustrated in Figure 2d.

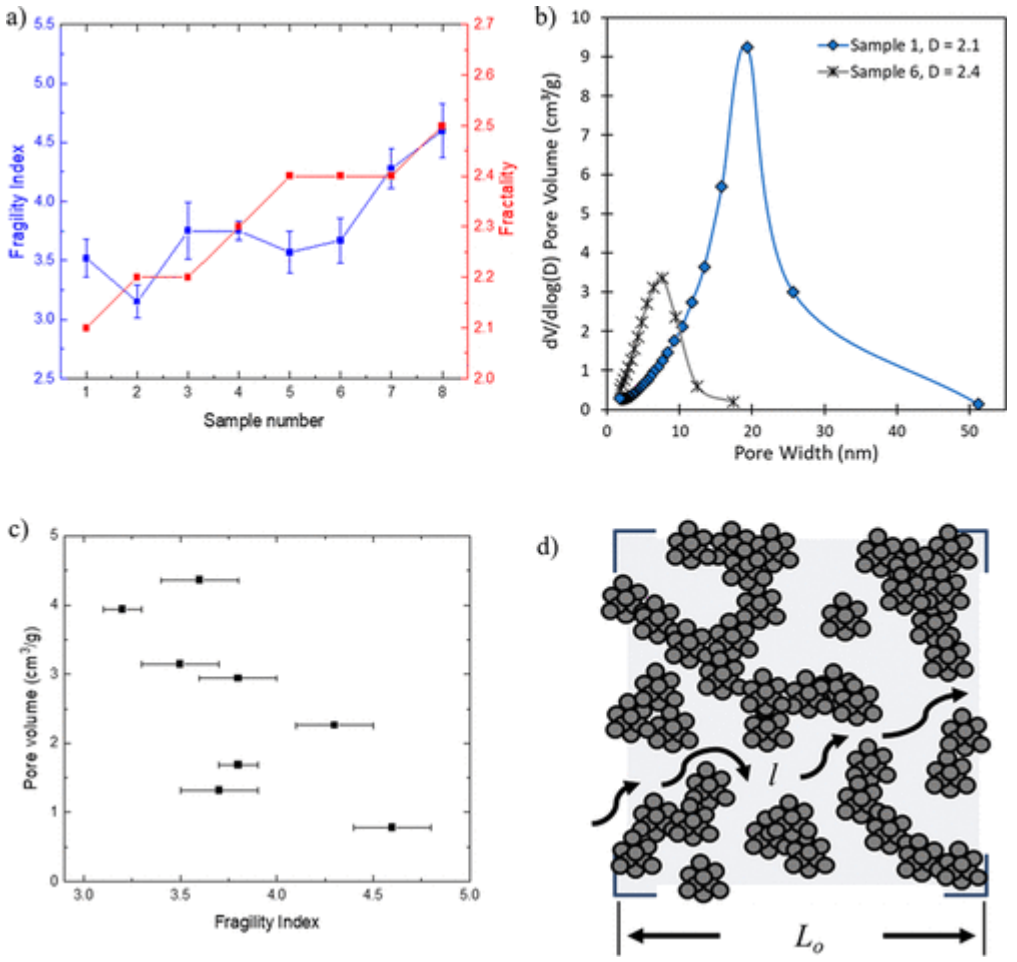

Figure 2. (a) Fragility index and mass fractal dimension shown for each sample, demonstrating a correlation between fragility and fractal dimension. (b) Pore size distributions for representative ionogel matrices; samples with high fractal dimensions exhibit smaller pore size distributions and high surface areas to satisfy a complex distribution of mass in the microstructure. (c) Fragility index as a function of specific pore volume demonstrates that highly porous samples tend toward a lower index. (d) Illustration of a tortuous conduction pathway due to the matrix; increasing the complexity of the matrix increases the conduction path length.

This analysis enables us to identify a design rule for increasing the conductivity of ionogels, that is, by increasing the pore volume, the fragility index decreases (Figure 2c), leading to a corresponding increase in mobility and conductivity. The latter is shown in Figure 3.

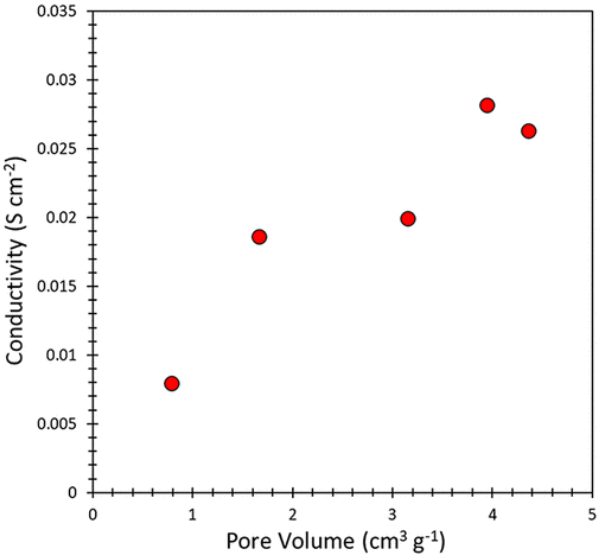

Figure 3. Ionic conductivities for silica ionogel samples as a function of the total pore volume. Increasing the pore volume creates a more open microstructure, increasing the degree of bulk ion transport and thus increasing mobility and conductivity for these samples by an order of magnitude.

The results also enable us to identify the interrelationships among fragility, conductivity, and microstructure by considering interactions which occur on the nanoscale level. Prior NMR results indicate that ionogels exhibit two distinct populations related to ion transport. There is a bulk fraction, several ionic radii away from the silica network, which exhibits mobilities comparable to the ionic liquid electrolyte and a surface fraction which exhibits restricted diffusion resulting from interactions of the ions with the silica surface. (35) Thus, we expect that the silica-based ionogels with greater levels of microporosity and, correspondingly, higher surface area will have lower conductivity. To evaluate this hypothesis, we characterize our pore size distribution in terms of the fraction of pores with diameters < 2 nm. Depending upon the specific ionogel sample, this microporosity fraction ranges between 0% and 50% as shown in Table 1. The relationship between microporosity fraction and surface area (Figure 4a) indicates that we can expect higher macroscale averaged interaction between the ionic liquid electrolyte and the silica network to occur with increasing levels of microporosity.

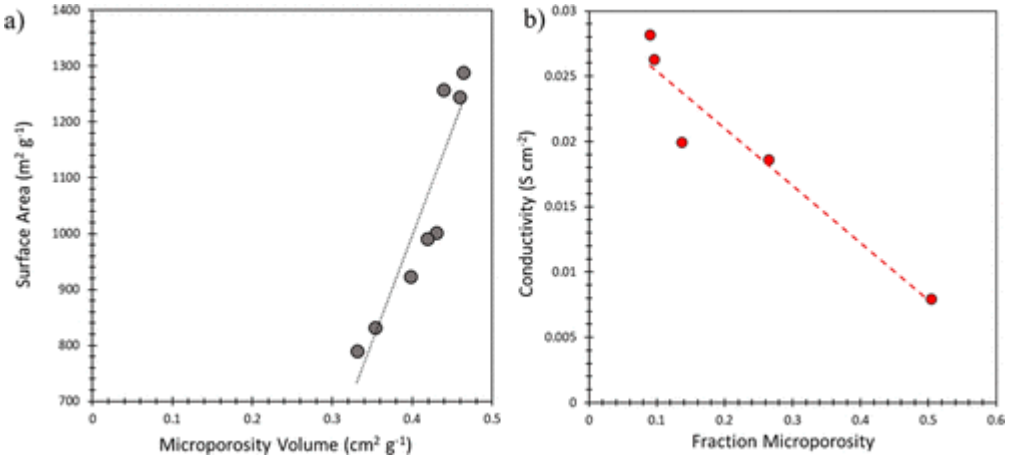

Figure 4. (a) Effect of microporosity on surface area, indicating that interfaces between the silica surface increase by a factor of 2 with higher microporosity volumes. (b) As the fraction of microporosity increases, there is restricted diffusion resulting from the interaction of ions with the silica surface, thus resulting in an order of magnitude decrease in ionic conductivity.

The microporosity variations result in two significant effects. First, we note that the conductivity decreases with increasing microporosity (Figure 4b), an indication that more of the ionic liquid electrolyte is confined at the pore walls, leading to lower overall conductivity. Related to this behavior is that greater levels of microporosity lead to lower macroscale molecular diffusion. Thus, the fragility increases with increasing microporosity (see Supporting Information S6).

As indicated in eq 5, conductivity as a function of porosity can also be represented analytically. Previous work on porous rock systems utilizing Archie's law was able to detail the effect of tortuosity on conductivity for porosity fractions up to $\varphi = 0.5$. (20,36−39) Extending this analysis to ionogels, Figure 5a relates conductivity to percent porosity, $(1 - \rho/\rho o) \times 100$, by plotting for a given temperature (in this case 80 °C) and highlighting the effect of the different ambigel samples. The cementation exponent of

3.04, which is the theoretical limit for very complex pathways, represents the total effect of the matrix on tortuosity, which is comprised of contributions from the mass fractal dimension and the random walk fractal dimension. These two fractal dimension contributions are associated with the complexity of the matrix microstructure and the complexity of a random walker pathway, respectively. The random walk fractal dimension is related to the mass fractal dimension with added contributions from the nature of the pore fluid and the fluid–matrix interface.

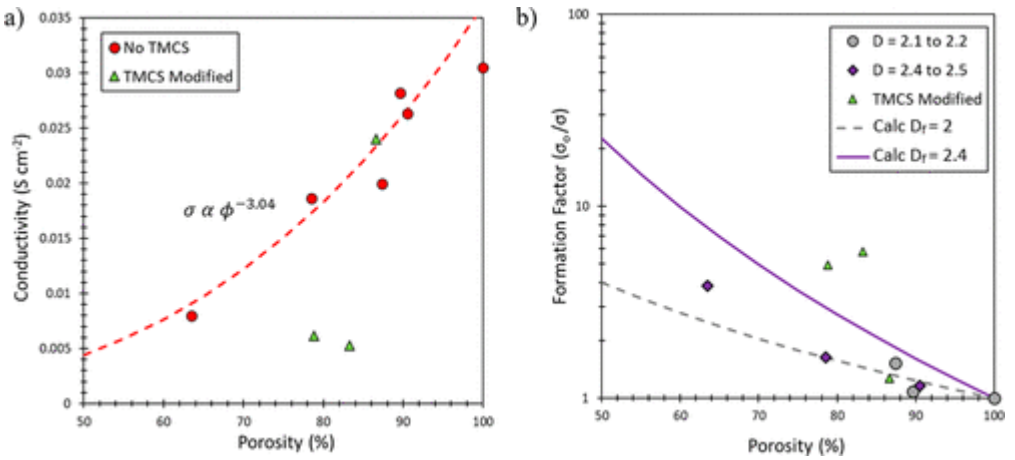

Figure 5. Effect of matrix porosity for silica and TMCS-modified silica on (a) the ionogel conductivity fit to Archie's Law using eq 4 and (b) the formation factor, calculated from boundary conditions for matrix complexity (fractal dimensionality), which both vary by a factor of 10.

We also normalized the results in terms of the formation factor (Figure 5b.). In this case, we apply Archie's law as expressed in eq 5 with the tortuosity (eq 6) for Df = 2.0 and Df = 2.5, which represent the boundary conditions for complexity in the ionogel microstructure. The TMCS-modified samples represent a special case where the random walk fractal dimension is increased by modifying the surface chemistry. The random walk dimension could be calculated for ionogels with a homogeneous silica matrix by using a simplified relationship between Df and Dw (see Supporting Information S2). Interestingly, the data does not seem to vary with respect to the fractal dimension for φ > 0.5. On the basis of eq 7, samples of greater complexity should demonstrate a more pronounced interaction with the matrix, as depicted by the solid and dashed lines in Figure 5b. However, given the extremely open microstructure of the silica network, the data show a trend located between the two limits and are indistinguishable for this sample set.

Finally, it is significant to highlight a few samples that further emphasize how surface interactions contribute to the conductivity behavior by examining the effect of a heterogeneous surface chemistry. Because samples 6 and 7 show similar fractal dimensions and surface area, one might expect that the higher porosity for sample 7 would result in higher conductivity and fragility. However, the addition of TMCS in sample 7 shifts the chemistry of the system from hydrophilic to hydrophobic, decreasing the ionic conductivity.

Figure 5a shows that the TMCS surface modification dramatically lowers the conductivity in ionogels. By modifying the surface chemistry of the matrix, one fills the micropore space with immobile species, modifying possible electrostatic interaction of ions with pore walls as well as reducing the number of distinct sites available for a random walker. Building from the concept outlined by Rammal and Toulouse (Supporting Information S2), we know that the number of available sites located within radius RN should scale with the number of steps taken by the walker (26)

$$G(N) \approx R_N^{D_F} \approx N^{D_S} \tag{10}$$

Therefore, by decreasing the number of sites available, the TMCS modification decreases the number of steps that can be taken, thus effectively decreasing the conductivity. Yet even for the TMCS modified samples, physical interactions at the interface as well as pore volume are the dominating factors regarding overall conductivity, as exemplified with sample 3, where the high pore volume still results in a high conductivity (Figure 3). With these design parameters in mind, we find that the conductivities for samples 2, 3, and 5 all approach that of unconfined ionic liquid.

Conclusions

The present study identifies several features of ionogel microstructures whose performance as a pseudosolid electrolyte is characterized in terms of the fragility and the conductivity of the ionogel. We establish a positive correlation between the fragility index, which characterizes, at the macroscale, the mobility of molecules in the pore fluid in each sample, and the mass fractal dimension, which describes the complexity of the microstructure. This relationship indicates that the mobility of the IL was

disrupted by the presence of the microporosity, and a more complex matrix results in lower macroscale molecular diffusion in the IL. Our results indicate that interaction between the ionogel electrolyte and the silica network affects the conductivity with high levels of microporosity increasing the surface area and leading to lower overall conductivity. A second important contribution comes from Archie's law analysis, where we obtained a power law relationship between porosity and conductivity as the cementation index of 3 corresponds to a high degree of tortuosity. (19) Taken together, our results show that ionogels with large porosities and low interface area will minimize the tortuosity for ionic conduction and lead to higher conductivity. This consideration translates to ionogel systems with low values of fragility indices and smaller fractal dimensions.

Acknowledgments

This research was supported in part by the U.S. Department of Energy Advanced Research Projects Agency-Energy (ARPA-E) Single-Pane Highly Insulating Efficient Lucid Designs (SHIELD) program (ARPA-E Award DE-AR0000738) and the NRT-INFEWS: Integrated Urban Solutions for Food, Energy, and Water Management (Grant No. DGE-1735325).

References

(1) Le Bideau, J.; Ducros, J.-B.; Soudan, P.; Guyomard, D. Solid- State Electrode Materials with Ionic-Liquid Properties for Energy Storage: the Lithium Solid-State Ionic-Liquid Concept. Adv. Funct. Mater. 2011, 21 (21), 4073−4078.

(2) Néouze, M.-A.; Le Bideau, J.; Leroux, F.; Vioux, A. A route to heat resistant solid membranes with performances of liquid electrolytes. Chem. Commun. 2005, 1082−1084.

(3) Néouze, M.-A.; Le Bideau, J.; Vioux, A. Versatile heat resistant solid electrolytes with performances of liquid electrolytes. Pro. Sol. State Chem. 2005, 33 (2), 217−222.

(4) Tan, G.; Wu, F.; Zhan, C.; Wang, J.; Mu, D.; Lu, J.; Amine, K. Solid-State Li-Ion Batteries Using Fast, Stable, Glassy Nanocomposite. Nano Lett. 2016, 16, 1960−1968.

(5) Guyomard-Lack, A.; Said, B.; Dupre, N.; Galarneau, A.; Le Bideau, J. Enhancement of lithium transport by controlling the mesoporosity of silica monoliths filled by ionic liquids. New J. Chem. 2016, 40, 4269−4276.

(6) Ashby, D. S.; Choi, C. S.; Edwards, M. A.; Talin, A. A.; White, H. S.; Dunn, B. S. High-Performance Solid-State Lithium-Ion Battery with Mixed 2D and 3D Electrodes. ACS Appl. Ener. Mater. 2020, 3 (9), 8402−8409.

(7) Zhang, S.; Zhang, J.; Zhang, Y.; Deng, Y. Nonconfined Ionic Liquids. Chem. Rev. 2017, 117, 6755−6833.

(8) DeBlock, R. H.; Wei, Q.; Ashby, D. S.; Butts, D. M.; Whang, G. J.; Choi, C. S.; Dunn, B. S. Siloxane-Modified, Silica-Based Ionogel as a Pseudosolid Electrolyte for Sodium-Ion Batteries. ACS Appl. Ener. Mater. 2021, 4 (1), 154−163.

(9) Ashby, D. S.; DeBlock, R. H.; Lai, C.-H.; Choi, C. S.; Dunn, B. S. Patternable, Solution-Processed Ionogels. Joule 2017, 1, 344−358.

(10) Ashby, D. S.; DeBlock, R. H.; Choi, C. S.; Sugimoto, W.; Dunn, B. S. Electrochemical and Spectroscopic Analysis of the Ionogel- Electrode Interface. ACS Appl. Mater.and Inter. 2019, 11, 12088− 12097.

(11) Guyomard-Lack, A.; Delannoy, P.-E.; Dupre, N.; Cerclier, C. V.; Humbert, B.; Le Bideau, J. Destructuring ionic liquids in ionogels: enhanced fragility for solid devices. Phys. Chem. Chem. Phys. 2014, 16, 23639−23645.

(12) Le Bideau, J.; Viau, L.; Vioux, A. Ionogels, ionic liquid based hybrid materials. Chem. Soc. Rev. 2011, 40, 907−925.

(13) Endres, F.; MacFarlane, D.; Abbott, A.Electrodeposition from Ionic Liquids; Wiley-VCH Verlag GmbH & Co. KGaA, 2017.

(14) Wang, X.; Hao, J. Recent advances in ionic liquid-based electrochemical biosensors. Sci. Bull. 2016, 61, 1281−1295.

(15) Angell, C. A. Relaxation in liquids, polymers and plastic crystals strong/fragile patterns and problems. J. of Non-Crys. Sol. 1991, 131−133, 13−31.

(16) Angell, C. A. Formation of Glasses from Liquids and Biopolymers. Science. 1995, 267 (5206), 1924−1935.

(17) Mauro, N. A.; Blodgett, M.; Johnson, M. L.; Vogt, A. J.; Kelton, K. F. A structural signature of liquid fragility. Nat. Commun. 2014, 5, 4616.

(18) Schaefer, D. W. Fractal models and the structure of materials. MRS Bull. 1988, 13 (2), 22−27.

(19) Ghanbarian, B.; Hunt, A. G.; Ewing, R. P.; Sahimi, M. Tortuosity in Porous Media: A Critical Review. Soil Sci. Soc. of Am. 2013, 77, 1461−1477.

(20) Wei, W.; Cai, J.; Hu, X.; Han, Q. An electrical conductivity model for fractal porous media. Geophys. Res. Lett. 2015, 42, 4833− 4840.

(21) Han, T.; Yan, H.; Fu, L. A quantitative interpretation of the saturation exponent in Archie's equations. Pet. Sci. 2021, 18, 444− 449.

(22) Majid, I.; Ben-Avraham, D.; Havlin, S.; Stanley, E. H. Exactenumeration approach to random walks on percolation clusters in two dimensions. Phys. Rev. B 1984, 30 (3), 1626−1628.

(23) Havlin, S.; Ben-Avraham, D. Diffusion in disordered media. Adv. Phys. 1987, 36 (6), 695−798.

(24) Dasgupta, R.; Ballabh, T.K.; Tarafdar, S. Distinct sites visited in a random walk on Sierpinski carpets. Phys. Lett. A 1994, 187 (1), 71− 73.

(25) Seeger, S.; Franz, A.; Schulzky, C.; Hoffmann, K. H. Random walks on finitely ramified Sierpinski carpets. Comput. Phys. Commun. 2001, 134 (3), 307−316.

(26) Rammal, R.; Toulouse, G. Random walks on fractal structures and percolation clusters. J. de Phys. Lett. 1983, 44 (1), 13−22.

(27) Wheatcraft, S. W.; Tyler, S. W. An explanation of scaledependent dispersivity in heterogeneous aquifers using concepts of fractal geometry. Wat. Resour. Res. 1988, 24 (4), 566−578.

(28) Bo-Ming, Y. Fractal character of tortuous streamtubes in porous media. Chi. Phys. Lett. 2005, 22, 158−160.

(29) Mandelbrot, B. B.The Fractal Geometry of Nature; Freeman: New York, 1983.

(30) Butts, D. M.; McNeil, P. E.; Marszewski, M.; Lan, E.; Galy, T.; Li, M.; Kang, J. S.; Ashby, D. S.; King, S.; Tolbert, S. H.; et al. Engineering mesoporous silica for superior optical and thermal properties. MRS Energy Sustainability 2020, 7, 39.

(31) Thommes, M.; Kaneko, K.; Neimark, A. V.; Olivier, J. P.; Rodriguez-Reinoso, F.; Rouquerol, J.; Sing, K. S. W. Physisorption of gases, with special reference to the evaluation of surface area and pore size distribution (IUPAC Technical Report). Pure Appl. Chem. 2015, 87 (9−10), 1051−1069.

(32) Beaucage, G. Approximations leading to a unified exponential/ power-law approach to small-angle scattering. J. of Appl. Crystall. 1995, 28, 717−728. The Journal of Physical Chemistry C pubs.acs.org/JPCC Article https://doi.org/10.1021/acs.jpcc.2c05911 J. Phys. Chem. C 2022, 126, 18528−18535 18534

(33) Beaucage, G. Small-angle scattering from polymeric mass fractals of arbitrary mass-fractal dimension. J. of Appl. Crystall. 1996, 29, 134−146.

(34) Jaroniec, M. Evaluation of the fractal dimension from a single adsorption isotherm. Langmuir 1995, 11, 2316−2317.

(35) Jayakody, N. K.; Fraenza, C. C.; Greenbaum, S. G.; Ashby, D.; Dunn, B. S. NMR Relaxometry and Diffusometry Analysis of Dynamics in Ionic Liquids and Ionogels for Use in Lithium-Ion Batteries. Jour. of Phys. Chem. B 2020, 124 (31), 6843−6856.

(36) Katz, A. J.; Thompson, A. H. Fractal sandstone pores: Implications for conductivity and pore formation. Phys. Rev. Lett. 1985, 54 (12), 1325−1328.

(37) Nigmatullin, R. R.; Dissado, L. A.; Soutougin, N. N. A fractal pore model for Archie's law in sedimentary rocks. J. of Phys. D: Appl. Phys. 1992, 25 (1), 32−37.

(38) Roy, S.; Tarafdar, S. Archie's law from a fractal model for porous rocks. Phys. Rev. B 1997, 55 (13), 8038−8041.

(39) Ruffet, C.; Gueguen, Y.; Darot, M. Rock conductivity and fractal nature of porosity. Terra Nova. 1991, 3 (3), 265−275.